


RESEARCH ARTICLE

Laser Desorption Ionization Quadrupole Ion Trap Time-of-Flight Mass Spectrometry of $Au_mFe_n^{+/-}$ Clusters Generated from Gold-Iron Nanoparticles and their Giant Nanoflowers. Electrochemical and/or Plasma Assisted Synthesis

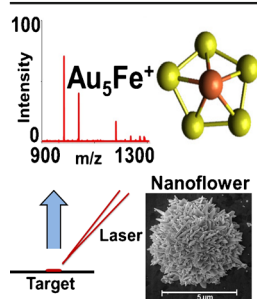
Ravi Madhukar Mawale,¹ Mayuri Vilas Ausekar,¹ David Pavlišák,^{2,3} Oleksandr Galmiz,^{2,3} Pavel Kubáček,¹ Josef Havel^{1,4} 

¹Department of Chemistry, Faculty of Science, Masaryk University, Kamenice 5/A14, 625 00, Brno, Czech Republic

²Department of Physical Electronics, Faculty of Science, Masaryk University, Kotlářská 2, 611 37, Brno, Czech Republic

³CEPLANT, R&D Center for Low-Cost Plasma and Nanotechnology Surface Modifications, Masaryk University, Kotlářská 2, 611 37, Brno, Czech Republic

⁴International Clinical Research Center, St. Anne's University Hospital, Pekařská 53, 656 91, Brno, Czech Republic



Abstract. Gold nanoparticles (NP) with average diameter ~100 nm synthesized from tetrachloroauric acid solution using stainless steel as a reducing agent were found to contain iron. Applying simultaneously high frequency (HF) plasma discharge in solution during the electrochemical reduction, giant gold-iron nanoflowers with average size ~1000–5000 nm were formed. Scanning electron microscopy (SEM) shows the morphology of the nanopowders produced as polygonal yet nearly spherical, whereas iron content in both products determined by energy dispersive X-ray analysis (EDX) was found to be at ~2.5 at. %. Laser desorption ionization (LDI) of both nanomaterials and mass spectrometric analysis show the formation of $Au_mFe_n^{+/-}$ ($m = 1-35$; $n = 1-3$) clusters. Structure of few selected clusters in neutral or

monocharged forms were computed by density functional theory (DFT) calculations and it was found that typical distances of an iron nucleus from adjacent gold nuclei lie in the interval 2.5 to 2.7 Å. Synthesized Au-Fe nanoparticles were found stable for at least 2 mo at room temperature (even in aqueous solution) without any stabilizing agent. Produced Au-Fe nanoparticles in combination with standard MALDI matrices enhance ionization of peptides and might find use in nanomedicine.

Keywords: Mass spectrometry, Nanoparticles, Nanoflowers, Plasma-assisted, Stainless steel, Laser desorption ionization

Received: 6 October 2016/Revised: 26 October 2016/Accepted: 28 October 2016/Published Online: 16 November 2016

Introduction

Metal nanoparticles (NPs) and nanostructures are on the forefront of various applications such as catalysis, sensing devices, optical devices, biomedicine, etc. The physical properties of metallic NPs may differ considerably from those

of the same bulk material [1, 2]. Gold NPs having large surface to volume ratio, unique optical, electronic properties, and easy surface modification have brought intensive focus for both research and industry [3]. The biocompatibility, resistance to oxidation, photo-bleaching immunity, and high contrast properties of the gold NPs are useful for the diagnosis and treatment of diseases as well as for selective drug delivery [4]. Gold nanostructures with different size and shape have also been used as substrate for the surface enhanced Raman spectroscopy [5–8]. Various methods for the synthesis of gold clusters have already been reported [9–12]. The properties of gold NPs can be greatly enhanced by mixing with other elements to generate

Electronic supplementary material The online version of this article (doi:10.1007/s13361-016-1547-1) contains supplementary material, which is available to authorized users.

Correspondence to: Josef Havel; e-mail: havel@chemi.muni.cz

bimetallic nanomaterials. For example, gold-iron (Au-Fe) bimetallic nanomaterials have stimulated great attention because of their potential applications in nanomedicine and nanotechnology. They are important for biomedical applications because of their supermagnetic behavior. The Au-Fe are expected to be superior than Au-Fe oxide nanomaterials because of high saturation magnetization of iron than iron oxide [13]. Several research groups have prepared and studied Au-Fe nanomaterials, but a large portion of these studies was focused on Au-Fe oxide core-shell structures. However, the core-shell particles have their own challenges [14–16].

Different approaches have been addressed for the synthesis of bimetallic NPs, for example, co-reduction [17], thermal decomposition [18, 19], and galvanic replacement reaction [20–22]. Synthesis of Au-coated iron [13, 23–25] or Au-coated iron oxide [26] core and shell nanostructures have been described. The synthesis of gold NPs using stainless steel as a reducing agent was already reported, but the presence of iron in formed gold NPs was not detected, perhaps because mass spectrometric study of this nanomaterial was not performed [27, 28].

Laser desorption ionization quadrupole ion trap time-of-flight mass spectrometry (LDI-QIT TOFMS) was found to be a powerful technique to follow the generation of clusters from various solid materials [29, 30]. In this paper, we have applied LDI-QIT TOFMS for detailed analysis of gold NPs synthesized electrochemically and/or using plasma discharge in solution, and we discovered the presence of iron in both the products.

Experimental

Chemicals

Tetrachloroauric acid (HAuCl₄), α -cyano-4-hydroxycinnamic acid (CHCA), trifluoroacetic acid (TFA), and acetonitrile were purchased from Sigma-Aldrich (Steinheim, Germany). Silicon wafer that was used for SEM, EDX, and XPS analyses was from ON Semiconductor Czech Republic s.r.o. (Rožnov pod Radhoštěm, Czech Republic), Stainless steel-ER 308LSi (iron 63%, chromium 20%, nickel 10%, manganese 1.8%) from Weld Profi s.r.o. (Brno, Czech Republic) was used as a reductant. Water (ultrapure) was double distilled from a quartz apparatus Heraeus Quarzschmelze (Hanau, Germany). Peptide calibration Mix 4 (PepMix 4) was purchased from LaserBio Labs (Sophia Antipolis, France). All the other reagents were of analytical grade purity. The PepMix 4MS kit contains five individual peptides (bradykinin fragment 1–5, angiotensin II human, neurotensin, adrenocorticotrophic hormone (ACTH) clip 18–39, and insulin bovine β -chain oxidized) covering the 500–3500 Da mass range.

Plasma Discharge

An experimental set-up is shown in the Figure 1a, b. The plasma was generated across a 5 mm gap between the surface

of 15 mL of 5 mM aqueous solution of HAuCl₄ and the quartz cuvette. The quartz cuvette served as the dielectric barrier, and it was filled with solution of oxalic acid (75 mS/cm) used as in [31] to increase the conductivity. Both electrically insulated solution volumes served as liquid electrodes for the dielectric barrier electrical discharge (DBD).

The power was supplied to the electrodes by the high voltage resonance generator Lifetech-300W (Brno, Czech Republic). Function generator GW-Instek SFG-2104 from Good Will Instrument Co., Ltd., (New Taipei City, Taiwan) was used to control frequency of HV generator pulses. The frequency of the pulse was in the 40–45 kHz range, in order to find the best resonance conditions. The power was controlled using a variable transformer and measured by a power meter, Orbit Merret OM 402 PWR (Praha, Czech Republic).

Mass Spectrometry

AXIMA Resonance mass spectrometer from Kratos Analytical Ltd. (Manchester, UK) was used to record the mass spectra in both positive and negative ion modes. The instrument was equipped with nitrogen laser (337 nm), quadrupole ion trap and time-of-flight mass analyzer. The quadrupole ion trap allows mass spectra to be recorded in selected m/z (mass-to-charge ratio) ranges: 100–400, 250–1200, 800–3500, 1500–8000, and 3000–1500. The laser repetition rate was set to 5 Hz with a pulse timer width of 3 ns. The laser power was expressed from 0 to 180 in arbitrary units (a.u.). The maximum laser power at 180 a.u. was 6 mW and the irradiated spot size was approximately 150 μ m in diameter. Mass spectra were obtained by accumulating spectra from at least 100 shots. Internal calibration of mass spectra in individual m/z ranges was performed using gold clusters generated simultaneously with Au_{*m*}Fe_{*n*} clusters. The advantage is that because gold is monoisotopic, the Au_{*m*}^{+/-} clusters show single peaks. Therefore, the use of gold clusters makes calibration easy and more precise. The mass accuracy achieved was below ± 20 mDa.

Scanning Electron Microscopy

A MIRA3 scanning electron microscope TESCAN (Brno, Czech Republic) was used for surface analysis. The instrument used in this study worked at a pressure of 0.0014 Pa in the chamber. The maximum spatial resolution was up to 1 nm at 30 kV, and the magnification was from 2 to 10⁶ times.

X-ray Photoelectron Spectroscopy

The surface chemical composition was determined by X-ray photoelectron spectroscopy (XPS) on an ESCALAB 250Xi electron spectrometer from Thermo Scientific (Leicestershire, UK). For the excitation of the photoelectron spectra, monochromatic Al K α and an analyzer pass energy of 20 eV was used. Charge neutralization was implemented by low energy electrons injected into the magnetic field of the lens from a filament located directly above the sample. Data acquisition

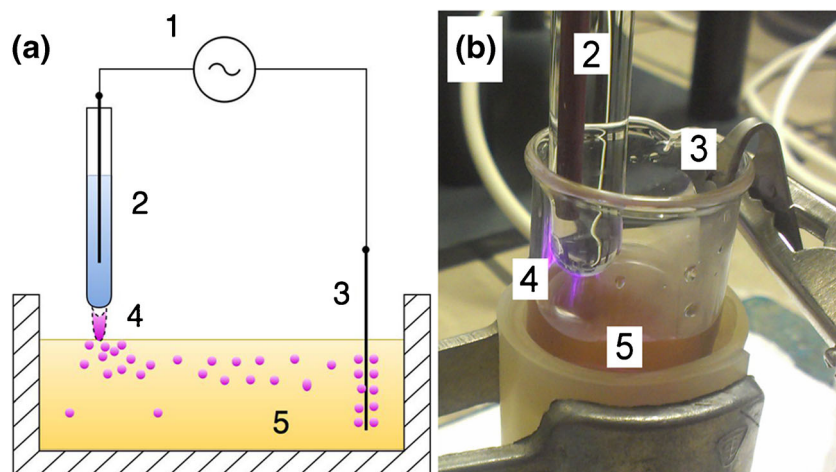


Figure 1. Scheme of the experimental assembly for the plasma-assisted synthesis of Au-Fe NPs (a), image taken of discharge at the discharge power 20 W (b). Items (1) HV generator, (2) glass cuvette with oxalic acid solution and steel electrode, (3) steel electrode, (4) plasma discharge, (5) HAuCl_4 solution

and processing were carried out using CasaXPS software, ver. 2.3.15 from Casa Software Ltd. (Leicestershire, UK). After subtraction of Shirley background, the peaks were fitted using Gaussian Lorentzian GL (30) peak shape. The binding energy (BE) was corrected for charging using an electron BE of 284.8 eV for the C 1s peak from residual carbon impurities. Similarly to SEM/EDX measurements, the samples for XPS experiments were prepared by nanoparticles film deposited on Si wafer.

Software and Computation

Theoretical isotopic patterns were calculated using Launchpad software (Kompact, ver. 2.9.3, 2011) from Kratos Analytical Ltd. (Manchester, UK). Examples of possible cluster structures were computed via DFT optimization using ADF 2013 and ADF 2014 molecular modeling suite [32, 33].

Stainless Steel Assisted Aynthesis of Gold-Iron NPs

Gold NPs were synthesized by reduction of HAuCl_4 using stainless steel as reducing agent at ambient conditions, similarly as in [27]. A piece of stainless steel rod was introduced into 5 mL of 5 mM HAuCl_4 aqueous solution and the reaction mixture was stirred using a magnetic bar for 60 min. After introduction of the stainless steel rod, the color of the solution changed from yellow to red. After 60 min of the reaction, the stainless steel rod was removed and the precipitate was washed several times with water and acetonitrile and then dried at ambient temperature (**Sample I**).

Plasma Assisted Aynthesis of Gold-Iron NPs

In this procedure, in addition to steel, an atmospheric pressure plasma was applied. It was observed that within some 20–30 s the color of the HAuCl_4 solution began changing from yellow to red, (first at the surface of solution), which indicated the formation of gold NPs. Simultaneously, there was formation of

red precipitate on the surface of iron electrode immersed into the tetrachloroauric acid solution. This means that two processes take place in parallel, one process in the solution due to the plasma action and the other one at the surface of the steel electrode. The formation of gold NPs at the surface of steel was faster than in the HAuCl_4 solution due to plasma. It is also assumed that the form of the created nanoparticles could also be influenced by the high frequency electric field. The red precipitate formed at the surface of the steel electrode was falling down into the solution. Therefore, **Sample II** was the mixture of products formed both in the solution and on the surface of the steel electrode.

Sample Preparation for Mass Spectrometric Analysis

The target plate was cleaned several times with ethanol and double distilled water and dried at room temperature before sample deposition. **Samples I–II** of isolated Au-Fe NP were washed with water and then with acetonitrile (as mentioned above). For MS analysis, 1 μL of acetonitrile suspension was deposited on the target plate and dried in a stream of air.

Results and Discussion

Scanning Electron Microscopy

The products formed in the redox process between HAuCl_4 and stainless steel with and without plasma were characterized by SEM analysis. The obtained NPs appear homogeneous in shape with polygonal yet nearly spherical geometry (Figure 2a). The NPs were well dispersed without aggregation and their average diameter was ~ 100 nm. SEM analysis shows that **Sample II** contains both NPs and nanoflowers, whereas red precipitate formed on the surface of the electrode (collected from the steel rod) during plasma assisted synthesis of Au-Fe NPs shows the formation of only giant gold nanoflowers

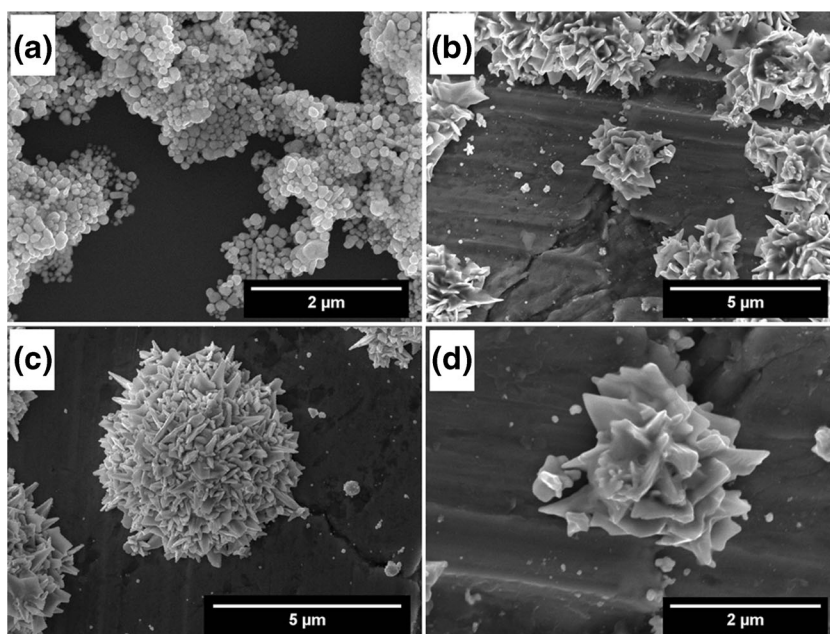


Figure 2. SEM images of gold-iron NPs **Sample I** (a), Au-Fe nanoflowers measured from the surface of the steel (under plasma treatment) in different forms and magnification (b), (c), and (d)

(Figure 2b). They consist of leaves, nanorods-like aggregates (Figure 2c), and leaves-based flowerlike structures (Figure 2d). The size of nanoflowers was found to be between 1000 and 5000 nm. It has been observed that prolonging the duration of plasma discharge does not alter significantly the size and shape of NPs and just increases the yield of the product.

The elemental composition of the **Samples I, II**, and red precipitate formed on the steel electrode was determined by EDX analysis and it is given in Table 1. It shows presence of iron (~2.5 at. %) in all the products with negligible amount of chromium and nickel.

X-ray Photoelectron spectroscopy

The **Samples I** and **II** were analyzed by the XPS, and no significant difference was been observed in the spectra. Lower values for Au/Fe ratio were obtained for XPS. It can be explained by the fact that XPS has much lower penetration depth [34]. The binding energies scale was calibrated taking as a reference the adventitious C 1s peak at 285 eV. A curve fitting procedure of the experimental spectra was done. As shown in Figure 3, deconvolution of Au 4f peak fits very well using three component models, respectively, at 83.8, 84.7, and 86.3 eV. According to the work in [35–39], the component at 83.8 eV indicates the presence of gold in the oxidation state Au⁰ (metallic state). XPS Au 4f peak deconvolution of AuFe nanoparticles is given in Table 1.

The components at higher BE at 84.7 and 86.3 eV were assigned to Au (I) and Au (III), respectively. In the Au 4f regions each gold species shows two peaks due to the Au 4f 7/2 and Au 4f 5/2 transitions (with chemical shift +3.65 eV). FWHM (full width half maximum) in all components does not exceed 0.7.

Mass Spectrometry

Mass spectra of **Sample I** were recorded in positive and negative ion mode with a mass resolution in the range 6000–10,000. The effect of laser energy on the ionization of mixed Au-Fe clusters was studied for each m/z range in both positive and negative ion mode. The threshold energy was determined to be in the range 100–120 a.u.

The effect of laser energy on the ionization of Au-Fe clusters in the range m/z 750–3500 is shown in Figure 4. The ionization of the Au_{*m*}Fe_{*n*} clusters increases by increasing the laser energy up to 140 a.u. but it decreases then with further increase the laser energy. The detailed analysis of the LDI mass spectrum recorded in positive ion mode is given in Figure 5 (m/z 180–1500) and Figure 6 (m/z 750–4000). The formation of various unary Au_{*m*} and binary Au_{*m*}Fe_{*n*} clusters is demonstrated. The general stoichiometry of the clusters was found to be Au_{*m*} ($m = 1–35$) and Au_{*m*}Fe_{*n*} ($m = 1–35$; $n = 1–2$). It was observed that gold clusters with odd number of atoms are more intensive than the gold clusters with even numbers, similarly detected by other authors for metallic clusters [40–42]. Few Au_{*m*}Cr_{*x*}⁺ and Au_{*m*}Fe_{*n*}Cr_{*x*}⁺ clusters of lower intensity were detected in higher range m/z 1500–8000. In addition, few

Table 1. Elemental Composition Measured by EDX and XPS Au 4f Peak Deconvolution of AuFe Nanoparticles

Samples	EDX [at. %]		XPS - Au 4f deconvolution [at. %]		
	Au	Fe	Au ⁰	Au ^{+I}	Au ^{+III}
Sample I	97.5	2.5	94.3	3.4	2.3
Sample II	97.6	2.4	91.9	6.1	2.0

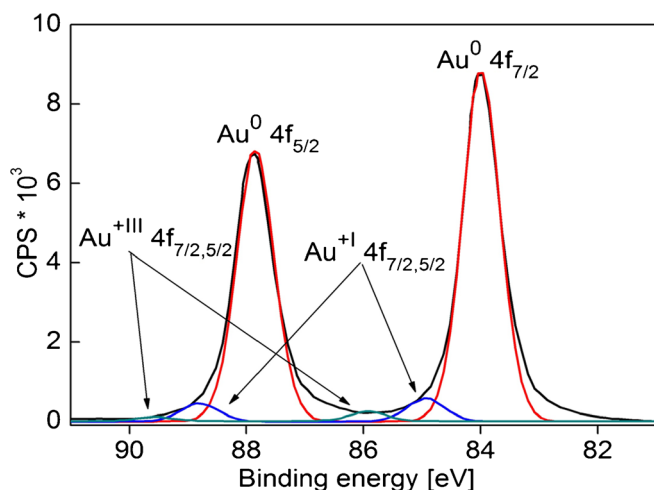


Figure 3. XPS of Au 4f obtained for **Sample II**. Au 4f spectrum (black) deconvoluted into three contributions: Au(0) (red), Au(I) (blue), and Au(III) (cyan). Background subtraction was done. **Sample I** gives almost identical spectra

hydrogenated and oxygenated clusters were also observed but they are minor species. Some chlorinated gold clusters (Figure 6, marked with asterisk) for example Au₈Cl⁺, Au₉Cl⁺, Au₁₀Cl⁺, Au₁₁Cl⁺, etc. and mixed Au_mFe_nCl_y^{+/-} clusters, for example Au₄FeCl⁺, Au₅FeCl⁺, Au₆FeCl^{+/-}, and Au₈FeCl^{+/-} were also detected. However, the intensities of Au_mFe_nCl_y^{+/-} and Au_mFe_nCl_y^{+/-} clusters are negligible (about 1% to 2% of those for Au_m clusters). The overview of clusters generated from **Sample I** is given in Table 2.

The clusters Au_m⁻ ($m = 1-6$) and few Au_mFe_n⁻ ($m = 3, 6; n = 1$) have been detected in the range m/z 100–1200. In higher range m/z 1200–8000, clusters Au_m⁻ ($m = 7-31$) and Au_mFe_n⁻ ($m = 7-31; n = 1-2$) were observed. Part of the spectrum in range m/z 1700–6500 is shown in Figure 7. Similarly like in positive ion mode, here some oxygenated, chlorinated gold, and mixed

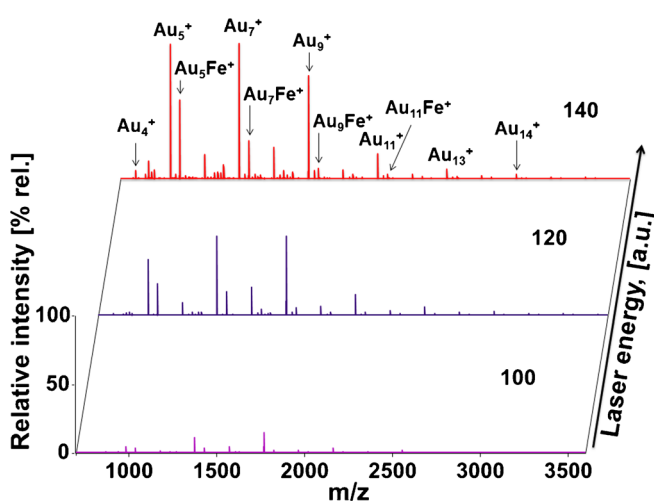


Figure 4. Mass spectra concerning LDI of the **Sample I** in range m/z 750–3500. Effect of laser energy. Mass spectra were normalized to 200 mV. Conditions: positive ion mode, laser energy 100–140 a.u.

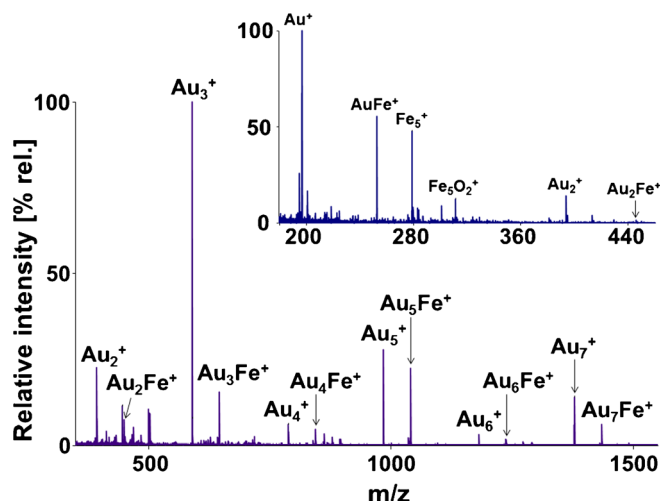


Figure 5. Mass spectrum of **Sample I** in the range m/z 0–1500. The mass spectrum in the range m/z 190–450 is given in the inset. Conditions: positive ion mode, laser energy 120 a.u.

Au_mFe_nCl_y⁻ clusters were also detected. In Figure 7 the peaks marked with an asterisk (*) correspond to Au_mCl_y⁻ clusters, for example Au₁₂Cl_y⁻, Au₁₄Cl_y⁻ etc. Few low intensive Au_mCr_x⁻ and Au_mFe_nCr_x⁻ clusters were detected in higher range m/z 1500–8000. The presence of a negligible amount of chromium in the Au-Fe nano-alloy was proven by EDX analysis. The source of chromium is stainless steel (Cr = 18% to 19%). The oxygenated species might be due to partial oxidation of iron and gold, whereas oxygen comes mostly from water.

Sample II was also analyzed by mass spectrometry (spectra are not given). The generation of Au_mFe_n clusters with n equal to 3 in both positive and negative ion modes has been observed. The general stoichiometry of the generated clusters was Au_mFe_n ($m = 1-35; n = 1-3$). In mass spectra of both the products (with and without using plasma), the intensities of

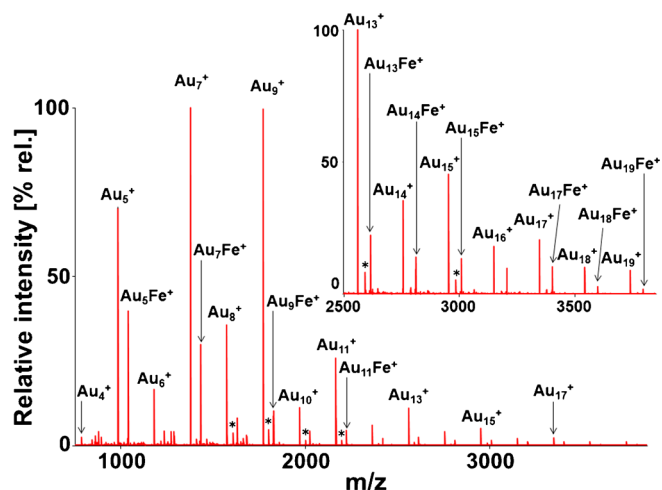


Figure 6. Mass spectrum of **Sample I** in the range m/z 750–4000. The magnification of mass spectrum in the range m/z 2500–4000 is given in the inset. Conditions: positive ion mode, laser energy 120 a.u. The peaks marked with * correspond to Au_mCl_y⁺ species

Table 2. Overview of the Stoichiometry of Au_mFe_n Clusters Generated by LDI of Au-Fe NPs in Positive and Negative Ion Mode. Observed $Au_m = 1-35$ clusters are omitted for the sake of clarity

Au_mFe_n clusters									
$AuFe^+$	$Au_2Fe^{+/-}$	$Au_3Fe^{+/-}$	Au_4Fe^+	$Au_5Fe^{+/-}$	$Au_6Fe^{+/-}$	$Au_7Fe^{+/-}$	$Au_7Fe_2^+$	$Au_8Fe^{+/-}$	$Au_9Fe^{+/-}$
$Au_{10}Fe^{+/-}$	$Au_{11}Fe^{+/-}$	$Au_{11}Fe_2^+$	$Au_{12}Fe^{+/-}$	$Au_{12}Fe_2^{+/-}$	$Au_{13}Fe^{+/-}$	$Au_{13}Fe_2^{+/-}$	$Au_{14}Fe^{+/-}$	$Au_{14}Fe_2^{+/-}$	$Au_{15}Fe^{+/-}$
$Au_{15}Fe_2^{+/-}$	$Au_{16}Fe^{+/-}$	$Au_{16}Fe_2^{+/-}$	$Au_{17}Fe^{+/-}$	$Au_{17}Fe_2^{+/-}$	$Au_{18}Fe^{+/-}$	$Au_{18}Fe_2^{+/-}$	$Au_{19}Fe^{+/-}$	$Au_{19}Fe_2^{+/-}$	$Au_{20}Fe^{+/-}$
$Au_{20}Fe_2^{+/-}$	$Au_{21}Fe^{+/-}$	$Au_{21}Fe_2^{+/-}$	$Au_{21}Fe_3^-$	$Au_{22}Fe^{+/-}$	$Au_{22}Fe_2^{+/-}$	$Au_{23}Fe^{+/-}$	$Au_{23}Fe_2^-$	$Au_{24}Fe^{+/-}$	$Au_{24}Fe_2^{+/-}$
$Au_{25}Fe^{+/-}$	$Au_{25}Fe_2^-$	$Au_{26}Fe^{+/-}$	$Au_{26}Fe_2^-$	$Au_{27}Fe^{+/-}$	$Au_{27}Fe_2^-$	$Au_{28}Fe^{+/-}$	$Au_{28}Fe_2^-$	$Au_{29}Fe^{+/-}$	$Au_{29}Fe_2^-$
$Au_{30}Fe^{+/-}$	$Au_{30}Fe_2^-$	$Au_{31}Fe^{+/-}$	$Au_{32}Fe^+$	$Au_{33}Fe^+$	$Au_{34}Fe^+$	$Au_{35}Fe^+$			

Note: The symbol '+/-' indicates that the species observed in both positive and negative ion mode; in bold there are possible endohedral structures, e.g., $Fe@Au_{14}$, etc

the peaks concerning Au_mFe_n clusters ($n = 2-3$) was lower than for clusters with $n = 1$.

The stoichiometry of the selected clusters was also confirmed by MS² analysis. For example, collision-induced dissociation (CID) of the cluster at m/z 1434.8 (Au_7Fe^+) leads to the formation of a product ion at m/z 1040.8 (Au_5Fe^+) corresponding to the loss of Au_2 (394.0 Da). The CID of cluster at m/z 1040.8 (Au_5Fe^+) leads to the formation of product ions at m/z 843.8 (Au_4Fe^+), 646.8 (Au_3Fe^+), and 590.8 (Au_3^+) with the loss of Au (197.0 Da), Au_2 (394.0 Da), and Au_2Fe (450.0 Da), respectively (Figure 8). Concluding, Au_4Fe^+ , Au_3Fe^+ , and Au_3^+ species generated during the fragmentation of Au_5Fe^+ cluster are giving some information about the structure of Au_5Fe^+ cluster. The fragmentation is in agreement with computed structures as shown in Figure 9.

Structure of Gold-iron Clusters

TOFMS does not provide direct structural information and thus it is difficult to evaluate the structures of Au-Fe clusters from the mass spectra alone. Some structures of Au-Fe clusters have already been reported [43–46], for example, $AuFe_2$, Au_2Fe , $AuFe_3$, Au_2Fe_2 , Au_3Fe [43]; $AuFe_5$, Au_2Fe_5 [44];

Au_nFe ($n = 1-6, 12$), Au_nFe_2 ($n = 1-4$), Au_nFe_3 ($n = 1-3$), Au_nFe_4 ($n = 1-2, 12$), $AuFe_5$ [45]; and Au_nFe ($n = 1-7$) [46]. Therefore, in this work, structures of Au_5Fe , Au_7Fe_2 , and Au_9Fe_2 clusters were computed as examples of higher clusters. The structure of clusters was designed by DFT optimization (ADF; scalar relativistic ZORA geometry optimization). The aim was to find few possible isomers with local minima for bonding energy. Therefore, kinetic stability by calculating saddle points was not investigated. The structures in local minima of potential energy surface always have iron atoms coordinated with several gold atoms (most often to 4–6) and possess few odd electrons (4–9). The typical distances of an iron nucleus from adjacent gold nuclei lie in the interval 2.5–2.7 Å (Figure 9). For the cluster Au_5Fe , the molecular geometry does not usually change much with the molecular charge. The structural differences between the mono-anionic and the corresponding neutral and mono-cationic moieties are within a few percent for bond length and angles. Calculations are needed to generalize the structural features of all the Au_mFe_n clusters, but are beyond the scope of this study.

Mechanism of the Redox Reaction When Using Steel

Different mechanisms have been proposed for the synthesis of gold NPs using stainless steel as reducing agent [27, 47].

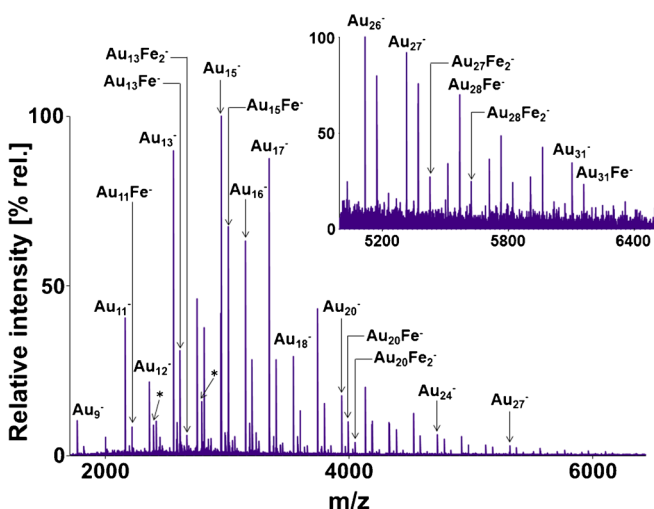


Figure 7. An example of mass spectrum from **Sample I** in the range m/z 1700–6500. The magnification of mass spectrum in range m/z 5000–6500 is given in the inset. Conditions: negative ion mode, laser energy 140 a.u. The peaks marked with * correspond to Au_mCl^- species

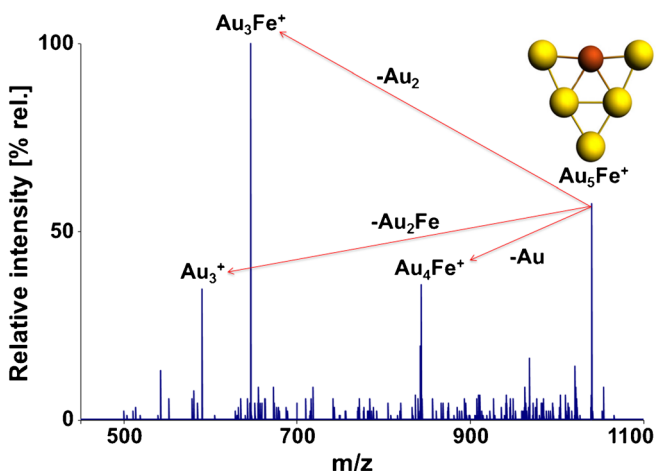


Figure 8. The MS² spectrum (for **Sample I**) concerning collision-induced dissociation (CID) of cluster at m/z 1040.8 [Au_5Fe^+] showing formation of product ions Au_3^+ , Au_3Fe^+ , and Au_4Fe^+ corresponding to the loss of Au_2Fe , Au_2 , and Au , respectively

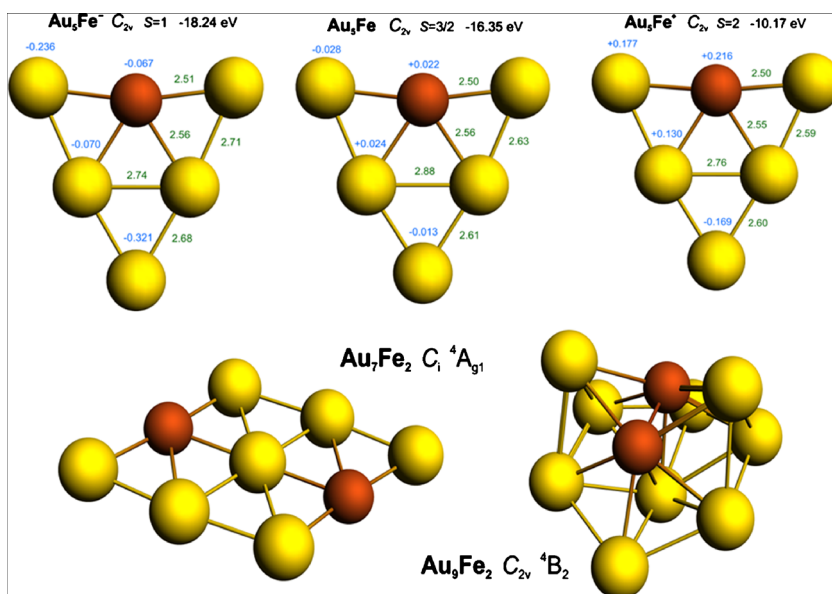


Figure 9. Structures of selected $Au_mFe_n^{+/-}$ clusters computed via DFT optimization using ADF® 2013 and ADF® 2014 molecular modeling suite

Stainless steel promotes the reduction of aqueous $HAuCl_4$ into gold NPs. The oxidation property of the tetrachloroauric acid might promote the oxidation of Fe (0) to Fe (II), and, simultaneously, reduction of gold from Au (III) to Au (0). As reported previously, the reduction of Au (III) is due to the electrons liberated during the oxidation of stainless steel Fe (0) to Fe (II) in higher amounts as well as other metals (Ni, Cr) to a lesser extent [27]. According to [48] the formation of metallic gold is reported as two step reaction. However, from mass spectra we cannot contribute to explain the mechanism.

Au-Fe NPs Assisted MALDI-TOFMS of Peptides

Synthesized Au-Fe NPs might have applications in medicine as for example drug carriers but also in mass spectrometry of biological samples. The use of prepared Au-Fe nano-material for so called “nanoparticles assisted MALDI TOF mass spectrometry” of peptides was examined here. We investigated the effect of Au-Fe NPs-enriched CHCA matrix on mass spectra of bradykinin, angiotensin II, neurotensin, ACTH, and insulin β -chain peptides commonly used for calibration in MS. The aqueous solution of PepMix 4 was made with addition of TFA (0.01%). The CHCA matrix (10 mg/mL) was prepared in acetonitrile/water (50/50 v/v) (0.1% TFA). Mass spectra of PepMix 4 standard using common α -cyano-4-hydroxycinnamic acid (CHCA) as a matrix were compared with those obtained for a mixture (CHCA matrix + Au-Fe NPs) and are given in Supplementary Figure S1. It is evident that combination of Au-Fe NPs and CHCA improves the intensities of bradykinin, angiotensin II, neurotensin, and ACTH peaks, namely 4.9, 56, 235, and 190 times, respectively. However, the peak intensity of the insulin β -chain decreased by 0.6 times compared with conventional CHCA matrix. Even with the addition of Au-Fe NPs at two different levels, no significant difference was observed, except for insulin β -chain,

where by using this Au-Fe nanomaterial we have obtained “better” results than those using flowerlike gold nanoparticles [49]. Most probably, the addition of Au-Fe NPs initiates growth of smaller and homogenous co-crystals of the matrix and the analyte as already described [49]. The use of Au-Fe NPs-enriched CHCA matrix provides higher resolution and, in most cases, significant increase of signal intensities of peptides, more so than with the conventional MALDI method.

Conclusions

In contrast to the literature, it was found that nano-gold prepared electrochemically using steel and tetrachloroauric acid is in reality gold-iron nanomaterial. Nanospheres, nanoleaves, and aggregates of the nanoleaves with nanorods-like objects and/or leaves-based giant nanoflowers under simultaneous HF plasma action are formed. Laser generated $Au_mFe_n^{+/-}$ (n max 3) clusters and quantum computation prove that the structure consists of max 1–3 atoms of iron surrounded by gold. These unique gold-iron nanoparticles are quite stable and when used in MALDI TOF MS they enhance highly the ionization of peptides. Easy and green synthesis of the nanoparticles and their properties might open new possibilities in bioanalytical applications.

Acknowledgments

The authors acknowledge support for this work by the Grant Agency of the Czech Republic (Project no.13-05082S), by the project R&D Centre for Low-Cost Plasma and Nanotechnology Surface Modifications CZ.1.05/2.1.00/03.0086 funding by the European Regional Development Fund, and also by the project LO1411 (NPU I) funded by the Ministry of Education Youth and Sports of Czech Republic.

References

- Chau, J.L.H., Chen, C.-Y., Yang, C.-C.: Facile synthesis of bimetallic nanoparticles by femtosecond laser irradiation method. *Arab. J. Chem.* In press (2013)
- Pazos-Pérez, N., Baranov, D., Irsen, S.: Synthesis of flexible, ultrathin gold nanowires in organic media. *Langmuir* **24**, 9855–9860 (2008)
- Zhang, Y., Chu, W., Foroushani, A., Wang, H., Li, D., Liu, J., Barrow, C., Wang, X., Yang, W.: New gold nanostructures for sensor applications: a review. *Materials* **7**, 5169–5201 (2014)
- Cornejo-Monroya, D.: Gold nanostructures in medicine: past, present and future. *J. Nanosci. Lett.* **3**, 1–9 (2013)
- Hong, S., Li, X.: Optimal size of gold nanoparticles for surface-enhanced Raman spectroscopy under different conditions. *J. Nanomater.* **2013**, 1–9 (2013)
- Quaresma, P., Osório, I., Dória, G., Carvalho, P.A., Pereira, A., Langer, J., Araújo, J.P., Pastoriza-Santos, I., Liz-Marzán, L.M., Franco, R., Baptista, P.V., Pereira, E.: Star-shaped magnetite@gold nanoparticles for protein magnetic separation and SERS detection. *RSC Adv.* **4**, 3659–3667 (2014)
- Quester, K., Avalos-Borja, M., Vilchis-Nestor, A.R., Camacho-López, M.A., Castro-Longoria, E.: SERS properties of different sized and shaped gold nanoparticles biosynthesized under different environmental conditions by *Neurospora crassa* extract. *PLoS One* **8**, 1–8 (2013)
- Morasso, C., Mehn, D., Vanna, R., Bedoni, M., Forvi, E., Colombo, M., Prospero, D., Gramatica, F.: One-step synthesis of star-like gold nanoparticles for surface enhanced Raman spectroscopy. *Mater. Chem. Phys.* **143**, 1215–1221 (2014)
- Zavras, A., Khairallah, G.N., O'Hair, R.A.J.: Gas phase formation, structure and reactivity of gold cluster ions. In: Mingos, D.M.P. (ed.) *Gold clusters, colloids and nanoparticles II* 162, 139–230. Springer International Publishing, Switzerland (2014)
- Pichugina, D.A., Kuz'menko, N.E., Shestakov, A.F.: Ligand-protected gold clusters: the structure, synthesis and applications. *Russ. Chem. Rev.* **84**, 1114–1144 (2015)
- Shichibu, Y., Suzuki, K., Konishi, K.: Facile synthesis and optical properties of magic-number Au₁₃ clusters. *Nanoscale* **4**, 4125–4129 (2012)
- Zhu, M., Lanni, E., Garg, N., Bier, M.E., Jin, R.: Kinetically controlled, high-yield synthesis of Au₂₅ clusters. *J. Am. Chem. Soc.* **130**, 1138–1139 (2008)
- Zhang, J., Post, M., Veres, T.: Laser-assisted synthesis of superparamagnetic Fe@Au core-shell nanoparticles. *J. Phys. Chem. B* **110**, 7122–7128 (2006)
- Lin, J., Zhou, W., Kumbhar, A., Wiemann, J., Fang, J., Carpenter, E.E., O'Connor, C.J.: Gold-Coated Iron (Fe@Au) Nanoparticles: synthesis, characterization, and magnetic field-induced self-assembly. *J. Solid State Chem.* **159**, 26–31 (2011)
- Ma, L., Borwankar, A., Willsey, B., Yoon, K., Tam, J., Sokolov, K., Feldman, M., Milner, T., Johnston, K.: Growth of textured thin Au coatings on iron oxide nanoparticles with near infrared absorbance. *Nanotechnology* **24**, 1–14 (2013)
- Tamer, U., Gündoğdu, Y., Boyacı, İ.H., Pekmez, K.: Synthesis of magnetic core-shell Fe₃O₄-Au nanoparticle for biomolecule immobilization and detection. *J. Nanoparticle Res.* **12**, 1187–1196 (2009)
- Link, S., Wang, Z.L., El-Sayed, M.A.: Alloy formation of gold-silver nanoparticles and the dependence of the plasmon absorption on their composition. *J. Phys. Chem. B* **103**, 3529–3533 (1999)
- Sun, S., Murray, C., Weller, D., Folks, L., Moser, A.: Monodisperse FePt nanoparticles and ferromagnetic FePt nanocrystal superlattices. *Science* **287**, 1989–1993 (2000)
- Dahal, N., Chikan, V., Jasinski, J., Leppert, V.: Synthesis of water-soluble iron-gold alloy nanoparticles. *Chem. Mater.* **17**, 6389–6395 (2008)
- Skrabalak, S., Chen, J., Sun, Y., Lu, X.: Gold nanocages: synthesis, properties, and applications. *Acc. Chem. Res.* **41**, 1587–1595 (2008)
- Xia, Y., Li, W., Copley, C., Chen, J.: Gold nanocages: from synthesis to theranostic applications. *Acc. Chem. Res.* **44**, 914–924 (2011)
- Mahmoud, M.A., El-Sayed, M.A.: Metallic double shell hollow nanocages: the challenges of their synthetic techniques. *Langmuir* **28**, 4051–4059 (2012)
- Langlois, C., Benzo, P., Arenal, R., Benoit, M., Nicolai, J., Combe, N., Ponchet, A., Casanove, M.J.: Fully crystalline faceted Fe-Au core-shell nanoparticles. *Nano Lett.* **15**, 5075–5080 (2015)
- Zhou, W., Carpenter, E., Lin, J., Kumbhar, A., Sims, J., O'Connor, C.J.: Nanostructures of gold coated iron core-shell nanoparticles and the nanobands assembled under magnetic field. *Eur. Phys. J. D.* **16**, 289–292 (2001)
- Chen, M., Yamamuro, S., Farrell, D., Majetich, S.A.: Gold-coated iron nanoparticles for biomedical applications. *J. Appl. Phys.* **93**, 7551–7553 (2003)
- Hien Pham, T.T., Cao, C., Sim, S.J.: Application of citrate-stabilized gold-coated ferric oxide composite nanoparticles for biological separations. *J. Magn. Magn. Mater.* **320**, 2049–2055 (2008)
- López-Lorente, A.I., Simonet, B.M., Valcárcel, M., Eppler, S., Schindl, R., Kranz, C., Mizaikoff, B.: Characterization of stainless steel assisted bare gold nanoparticles and their analytical potential. *Talanta* **118**, 321–327 (2014)
- López-Lorente, Á.I., Valcárcel, M., Mizaikoff, B.: Continuous flow synthesis and characterization of tailor-made bare gold nanoparticles for use in SERS. *Microchim. Acta* **181**, 1101–1108 (2014)
- Mawale, R.M., Amato, F., Alberti, M., Havel, J.: Generation of new Ag_mTe_n clusters via laser ablation synthesis using Ag-Te nano-composite as precursor. Quadrupole ion trap time-of-flight mass spectrometry. *Rapid Commun. Mass Spectrom.* **28**, 2753–2758 (2014)
- Mawale, R.M., Amato, F., Alberti, M., Havel, J.: Generation of Au_pAg_qTe_r clusters via laser ablation synthesis using Au-Ag-Te nano-composite as precursor: quadrupole ion-trap time-of-flight mass spectrometry. *Rapid Commun. Mass Spectrom.* **28**, 1601–1608 (2014)
- Pavliňák, D., Galmiz, O., Zemánek, M., Brablec, A., Čech, J., Černák, M.: Permanent hydrophilization of outer and inner surfaces of polytetrafluoroethylene tubes using ambient air plasma generated by surface dielectric barrier discharges. *Appl. Phys. Lett.* **105**, 154102 (2014)
- Te Velde, G., Bickelhaupt, F.M., Baerends, E.J., Fonseca Guerra, C., van Gisbergen, S.J.A., Snijders, J.G., Ziegler, T., Velde, G.T.E., Guerra, C.F., Gisbergen, S.J.A.V.A.N.: Chemistry with ADF. *J. Comput. Chem.* **22**, 931–967 (2001)
- Fonseca Guerra, C., Snijders, J.G., Te Velde, G., Baerends, E.J.: Towards an order-N DFT method. *Theor. Chem. Acc.* **99**, 391–403 (1998)
- Beamson, G., Briggs, D.: High resolution XPS of organic polymers: the scienta ESCA300 database. Wiley (1992)
- Salama, T.M., Shido, T., Minagawa, H., Ichikawa, M.: Characterization of gold(I) in NaY zeolite and acidity generation. *J. Catal.* **152**, 322–330 (1995)
- Epling, W.S., Hoflund, G.B., Weaver, J.F., Tsubota, S., Haruta, M.: Surface characterization study of Au/Fe₂O₃ and Au/Co₃O₄ low-temperature CO oxidation catalysts. *J. Phys. Chem.* **100**, 9929–9934 (1996)
- Park, E.D., Lee, J.S.: Effects of pretreatment conditions on CO oxidation over supported Au catalysts. *J. Catal.* **186**, 1–11 (1999)
- Visco, A.M., Neri, F., Neri, G., Donato, A., Milobe, C., Galvagno, S.: X-ray photoelectron spectroscopy of Au/FeO catalysts. *Phys. Chem. Chem. Phys.* **1**, 2869–2873 (1999)
- Minicò, S., Scirè, S., Crisafulli, C., Galvagno, S.: Influence of catalyst pretreatments on volatile organic compounds oxidation over gold/iron oxide. *Appl. Catal. B Environ.* **34**, 277–285 (2001)
- O'Hair, R.A.J., Khairallah, G.N.: Gas phase ion chemistry of transition metal clusters: production, reactivity, and catalysis. *J. Cluster Sci.* **15**, 331–363 (2004)
- Schweikhard, L., Hansen, K., Herlert, A., Herráiz Lablanca, M.D., Marx, G., Vogel, M.: Laser investigations of stored metal cluster ions. In: Knudsen, H., Andersen, J.U., Kluge, H.-J. (eds.) *Atomic physics at accelerators: Stored particles and fundamental physics*, pp. 275–281. Springer, Netherlands (2003)
- Teo, B.K., Zhang, H.: Magic numbers in clusters: Nucleation and growth sequences, bonding, principles, and packing patterns. In: Fedlheim, D.L., Foss, C.A. (eds.) *Metal nanoparticles: Synthesis, characterization, and applications*, p. 71. CRC Press, New York (2001)
- Melnik, M., Mikuš, P.: Structural characterization of heterometallic gold-iron clusters. *Int. Res. J. Pure Appl. Chem.* **5**, 273–317 (2015)

44. Rossell, O., Seco, M., Segalés, G., Pellinghelli, M.A., Tiripicchio, A.: Iron/gold carbide clusters containing Fe₅Au or Fe₅Au₂ skeletons: X-ray crystal structure of [Fe₅CAu₂(CO)₁₄(dppm)]. *J. Organomet. Chem.* **571**, 123–128 (1998)
45. Woldeghebriel, H.: Structures, energetics and magnetic properties of Au_nSFe_m and Au_nFe_m clusters for $m= 1-5$ and $n= 1-5, 12$ and 32 . *Momona Ethiop. J. Sci.* **6**, 73–94 (2014)
46. Die, D., Kuang, X.-Y., Guo, J.-J., Zheng, B.-X.: First-principle study of Au_nFe_e ($n=1-7$) clusters. *J. Mol. Struct. (THEOCHEM)* **902**, 54–58 (2009)
47. Han, T.H., Khan, M.M., Kalathil, S., Lee, J., Cho, M.H.: Synthesis of positively charged gold nanoparticles using a stainless-steel mesh. *J. Nanosci. Nanotechnol.* **13**, 6140–6144 (2013)
48. Moodley, K., Nicol, M.: Kinetics of reduction of gold (III) by platinum (II) and iron (III) in aqueous chloride solutions. *J. Chem. Soc. Dalt.* **26**, 3–6 (1977)
49. Kolářová, L., Kučera, L., Vaňhara, P., Hampl, A., Havel, J.: Use of flower-like gold nanoparticles in time-of-flight mass spectrometry. *Rapid Commun. Mass Spectrom.* **29**, 1585–1595 (2015)